Wide dynamic range microwave planar coupled ring resonator for sensing applications

Mohammad Hossein Zarifi, and Mojgan Daneshmand

Articles you may be interested in

Microbead-assisted high resolution microwave planar ring resonator for organic-vapor sensing
Applied Physics Letters **106**, 062903 (2015); 10.1063/1.4907944

Microfluidic metamaterial sensor: Selective trapping and remote sensing of microparticles
Journal of Applied Physics **121**, 023102 (2017); 10.1063/1.4973492

DNA sensing using split-ring resonator alone at microwave regime
Journal of Applied Physics **108**, 014908 (2010); 10.1063/1.3459877

Biosensing using split-ring resonators at microwave regime
Applied Physics Letters **92**, 254103 (2008); 10.1063/1.2946656

Asymmetric split-ring resonator-based biosensor for detection of label-free stress biomarkers
Applied Physics Letters **103**, 053702 (2013); 10.1063/1.4816440

Complex permittivity measurement using metamaterial split ring resonators
Journal of Applied Physics **121**, 054101 (2017); 10.1063/1.4975111

Wide dynamic range microwave planar coupled ring resonator for sensing applications

Mohammad Hossein Zarifi and Mojgan Daneshmand
Department of Electrical and Computer Engineering, University of Alberta, Edmonton, Alberta T6G 1H9, Canada

A highly sensitive, microwave-coupled ring resonator with a wide dynamic range is studied for use in sensing applications. The resonator's structure has two resonant rings and, consequently, two resonant frequencies, operating at 2.3 and 2.45 GHz. Inductive and capacitive coupling mechanisms are explored and compared to study their sensing performance. Primary finite element analysis and measurement results are used to compare the capacitive and inductive coupled ring resonators, demonstrating sensitivity improvements of up to 75% and dynamic range enhancement up to 100% in the capacitive coupled structure. In this work, we are proposing capacitive coupled planar ring resonators as a wide dynamic range sensing platform for liquid sensing applications. This sensing device is well suited for low-cost, real-time low-power, and CMOS compatible sensing technologies. *Published by AIP Publishing.* [http://dx.doi.org/10.1063/1.4953465]

Planar microwave resonator sensors have recently been employed in various sensing applications, demonstrating reliable, reproducible results. They have been used for bio-medical, industrial, safety, and security applications to detect small particles or pieces in various environments.[1–5] Planar-ring microwave resonator sensors have been used for liquid interface detection,[6] biomolecule detection in microfluidic channels,[7] and real-time DNA sensing[8] applications. Planar resonators also demonstrate promising results for gas and humidity sensing applications.[9–11] These resonators have been integrated with nanotube structures to study nanotube behavior when exposed to ultra-violet light[12] or to enhance the sensing performance of microwave resonators.[9,13]

While planar microwave resonator sensors have demonstrated promising performance as inexpensive, robust, contactless sensors, they suffer from problems like selectivity, low-resolution, and limited dynamic range.[14] To improve the resolution of planar resonator sensors, the quality factor must be improved. Lee *et al.* have reported a biocompatible, impedance-matched microwave planar resonator device with a quality factor of 1670.[1] Using active devices in microwave passive sensors has also been reported to increase the quality factor and resolution;[15–17] however, they require DC adjustment and calibration, which can be limiting parameters for active-loop assisted devices in applications such as implantable or wearable devices.[18]

Ring resonators have been widely used for sensing applications.[6] They offer moderate quality factors and could benefit from quality factor enhancement. It has been shown that coupling (inductive or capacitive) between planar microstrip resonators can increase the quality factor.[19]

In this paper, we present coupled ring resonator sensors and investigate their sensing performance in inductive and capacitive coupled forms. The design and analysis details are presented next, followed by measurements and discussions. Their sensitivity and dynamic range are studied and compared, with the capacitive coupled structure demonstrating a significant performance advantage over the inductive coupled one.

The sensing platform consists of two capacitive or inductive coupled planar microstrip ring-resonators, as shown in Fig. 1.[20] The operational principal for the presented sensors is based on permittivity and conductivity variations in the vicinity of the resonators' surface. Permittivity variations in the medium surrounding the sensor affect fundamental characteristics of the resonator such as its resonant frequency, quality factor, and resonant amplitude, which can be used to characterize material changes in close proximity to the resonator.

Table I summarizes the size specifications of the sensors as implemented in both capacitive and inductive coupling modes. In Fig. 1(a), the resonant ring is magnetically coupled to the input and output signal line while the two rings are electrically coupled to each other. For the inductive coupling structure (Fig. 1(b)), the two rings are magnetically coupled to each other while a capacitive coupling establishes a link to the signal input/output lines.

The resonant frequency for each ring structure can be calculated as: $f = c/(2 \times L \times \sqrt{\varepsilon_{eff}})$,[1] where c is the speed of light, L is the physical length of the ring and, and ε_{eff} is the effective permittivity of the near ambient of the resonator.[1] Since the length of the rings is equal, they have identical resonant frequencies in a given ambient permittivity. These rings are highly coupled in both capacitive and inductive coupled structures. This can lead to frequency splitting
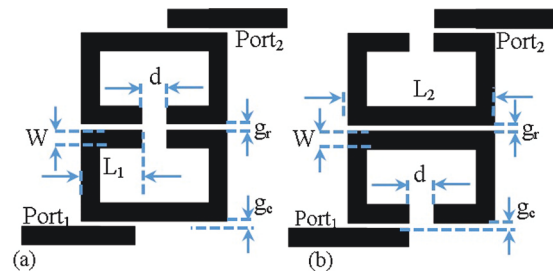

FIG. 1. Planar coupled resonator sensor structure: (a) capacitive coupling and (b) inductive coupling.

TABLE I. Designed ring resonator specifications in HFSS.

	W	g_r	g_c	d	L_1	L_2
Values (mm)	2.4	0.7	0.6	3	5.4	14

phenomena and creates a coupled resonator with two resonant frequencies in its frequency profile. The distance between two resonant frequencies in the resonance profile of each coupled resonator is adjustable by changing the structure parameters which control the coupling factor between the rings. Simulation results in Fig. 2 presents the effect of varying the coupling gap (g_r) between the rings on the resonant profiles of the presented structures in Fig. 1.

Considering the circuit models in Figs. 2(c) and 2(d), the resonant frequencies for the capacitive and inductive coupled resonators can be estimated as $f_{L/H} \approx 1/\sqrt{L_r(C_r \pm C_m)}$ and $f_{L/H} \approx 1/\sqrt{C_r(L_r \pm L_m)}$, respectively.[20] From these equations, it can be determined that increasing the coupling factor (C_m or L_m) can create frequency splitting for both capacitive and inductive coupled resonators as shown in Figs. 2(a) and 2(b).

In planar microwave resonator sensors, variations in the permittivity of the sensor-ambient are translated to sensor characteristics through alterations in the electric field. The electric field around the resonator is affected by the electrical permittivity and loss-factor (real and imaginary parts of the dielectric properties) of the carrier substrate and the materials above the resonator surface (material under test (MUT)). The simulated electric field distribution of the resonator within a distance of 2 mm above the surface of the resonators is presented in Fig. 3. The electric field is stronger in capacitive coupled regions than the other areas. These regions can be considered as hot-spots for the sensor, to be used as the most sensitive areas.

To verify the sensing capability of the proposed resonator structures, a simulation is run in HFSS software[21] with a material under test (MUT) placed in the hot spots of both resonators and the resulting S_{21}-parameter observed. Fig. 4 presents the simulated structure with the MUT on the sensitive areas. The S_{21}-parameter is investigated for variant

FIG. 3. HFSS simulations, studying the electric field concentration 2 mm above the surface of the capacitive and inductive coupled resonators. Capacitive coupled areas demonstrate higher field intensity than other regions.

MUT permittivities of 1–30 while the loss factor is considered to remain constant at zero (Figs. 4(c) and 4(d)). As clearly depicted in Fig. 4(c), high resonant frequencies (f_H) experience smaller variations than low resonant frequencies

FIG. 4. HFSS Simulation of resonant profile comparison between capacitive and inductive coupled resonators for an MUT of varying permittivity: (a) capacitive coupled, (b) inductive coupled, (c) S_{21} for capacitive coupled structure, and (d) S_{21} for inductive coupled structure.
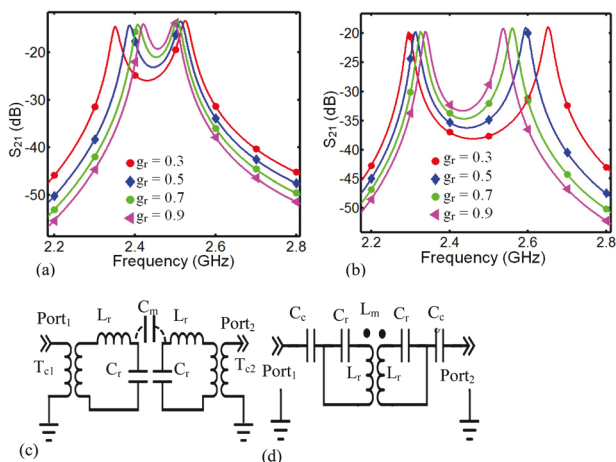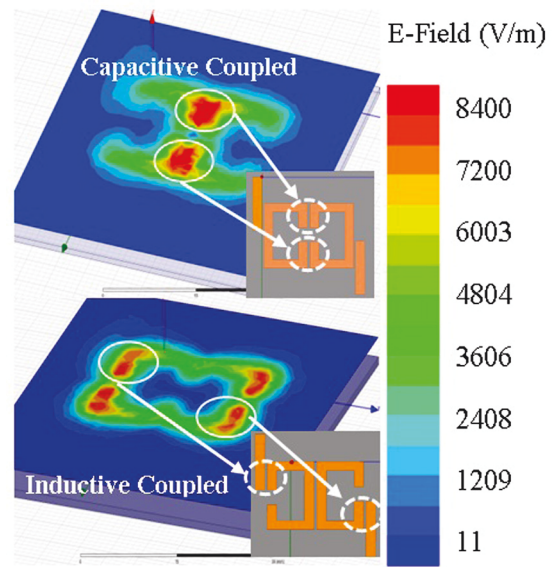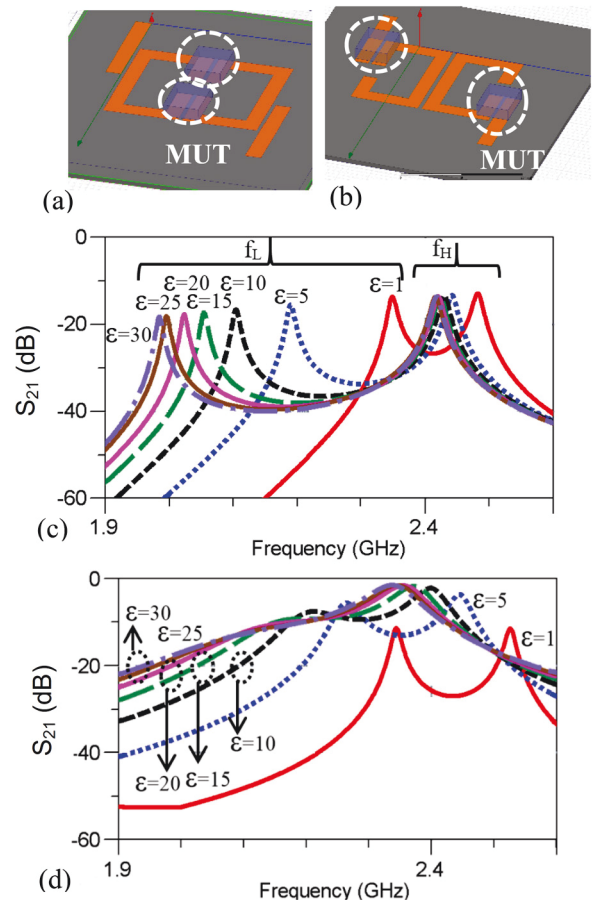

FIG. 2. Effect of varying coupling gap for (a) capacitive and (b) inductive coupled resonators. Circuit model for (c) capacitive and (d) inductive coupled structures with Advanced Design System (ADS) simulation.

(f_L) for the capacitive coupled structure. The correspondingly opposite trend is found in the inductive coupled resonator, where high resonant frequencies (f_H) experience larger variations than low resonant frequencies (f_L) and the response profile gets distorted.

Further investigations for f_L in capacitive coupling, and f_H in inductive coupling, are performed and presented in Fig. 5. According to the simulation results, the f_L in capacitive coupled resonator structures is more sensitive to permittivity variations than the f_H in the inductive coupled structures. Additionally, the quality factor of the resonance profile (resonant frequency over −3 dB bandwidth) in the capacitive coupled resonator demonstrates a 20% increase and remains constant while its corresponding value in the inductive coupled resonator drops tremendously (Figs. 5(a) and 5(b)). The resonators' responses to loss-factor variation are also studied at a constant permittivity of 2 and presented in Figs. 5(c) and 5(d). Incrementing the loss-factor from 0 to 0.2 results in a 0.5% variation in the resonant frequency for both capacitive and inductive coupled resonators. The quality factor of the resonance profile at the sensitive resonant frequency (f_L) of the capacitive coupled resonator sees a larger drop than the inductive coupled resonator at its sensitive resonant frequency (f_H) (Fig. 5(d)). From this figure, we see that the capacitive coupled resonator demonstrates twice the sensitivity to permittivity variations that the inductive coupled resonator for the same range of permittivity variation sees, with high and nearly constant quality factor. The frequency span for HFSS simulations is selected from 1 GHz to 3 GHz with the step size of 500 kHz and convergence target of 0.0002.

The proposed coupled resonators are fabricated on microwave substrates from Rogers Corporation (8550) with a dielectric thickness of 0.79 mm and permittivity of 2.2 ± 0.2. Copper layers with conductivity of 58 MS/m create microstrip traces and the ground layer beneath the microstrip lines. The implemented capacitive and inductive coupled resonators are presented in Fig. 6. To investigate their sensing performance, the electric field hot-spots (Fig. 3) are exposed to materials with different permittivities.
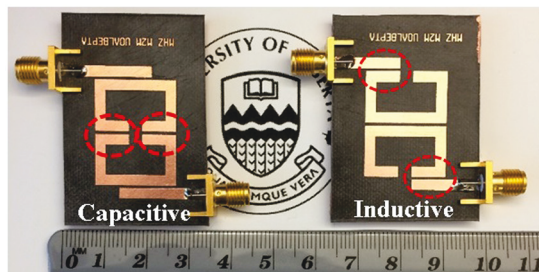
FIG. 6. Implemented capacitive and inductive coupled resonators to investigate and compare their dielectric sensing performance.

The initial measurements are performed using bare resonators (implemented resonators with no samples for sensing), which demonstrate low and high resonant frequencies of 2.29 GHz and 2.44 GHz for the capacitive coupled resonator, and 2.28 GHz and 2.46 GHz for the inductive coupled resonator (Fig. 7). To study the sensing performance of the resonators, two accurate 5880 substrate samples from Rogers Corporation, with permittivity of 2.2, loss-factor of 0.009, and of dimensions 7 mm × 7 mm with different thicknesses of 0.79 and 1.58 mm are used as the material under test. According to the measured results of the MUT with a thickness of 0.79 mm, the f_H inductive coupled resonator demonstrates 0.64% variation while the f_L capacitive coupled resonator has 1.96% variation for the same material with respect to the bare resonant frequencies.

The resonant frequency variation of inductive and capacitive coupled resonators is then measured for the MUT with thickness of 1.56 mm. The f_H with the MUT displays a 0.87% variation compared with the f_H of the bare resonant frequency inductive coupled resonator. The resonant frequency variation in f_L for the MUT is 2.48% in the capacitive coupled resonator. A comparison between the resonant frequency shift for inductive and capacitive coupled resonator illustrates that capacitive coupled resonator presents 200% more variation than the inductive coupled one.

Additional experiments with deionized water (DI) and high concentrations of sodium chloride (NaCl) in DI water (saline solution) are also performed to compare the sensing performance between capacitive and inductive coupled resonators. As Fig. 8 shows, (according to MUT configurations in Figs. 4(a) and 4(b)), for 20 μl of DI water, the second resonant frequency of the inductive coupled resonator disappears
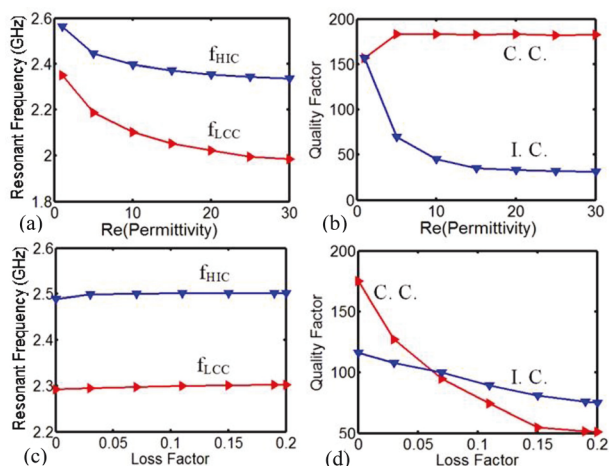

FIG. 5. Comparison of simulated capacitive (C.C) and inductive coupled resonators (I.C), (a) resonant frequency versus variant permittivity at zero loss-factor, (b) quality factor for the resonant frequencies versus variant permittivity at zero loss-factor, (c) resonant frequency versus variant loss-factor at permittivity of 2, and (d) quality factor versus variant loss-factor at permittivity of 2.
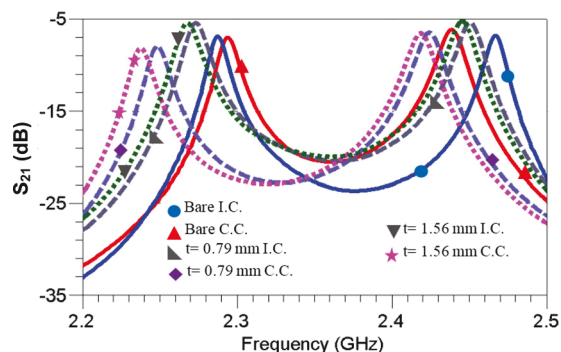

FIG. 7. Measured S_{21} parameters of the implemented resonators for bare and different MUTs with permittivity of 2.2 and dimensions of $7 \times 7 \times 0.79 \, mm^3$ and $7 \times 7 \times 1.56 \, mm^3$.
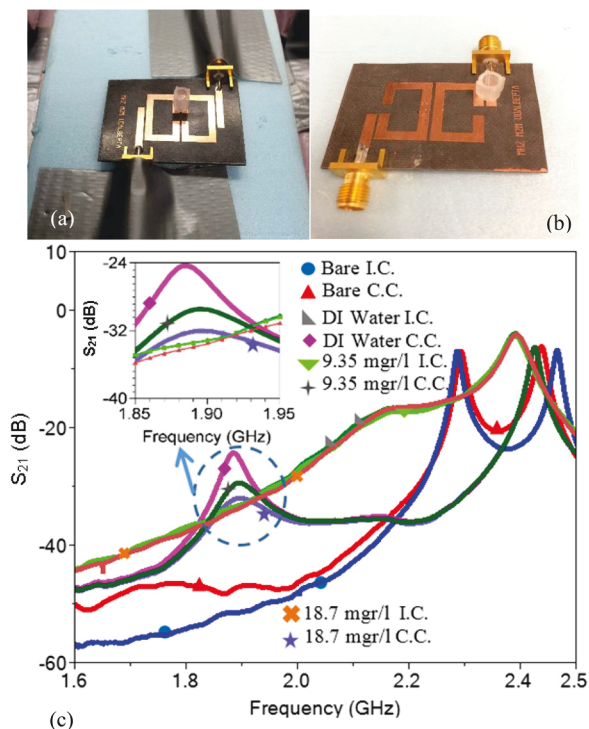
FIG. 8. (a) Implemented capacitive coupled ring resonator with liquid container, (b) inductive coupled ring resonators with liquid container, (c) measured S_{21}-parameter comparison between inductive coupled (I.C.) and capacitive coupled (C.C) resonator sensors for DI-water and different concentration of NaCl in DI-water.

(since the quality factor drops so tremendously), while the capacitive coupled resonator maintains its lower resonant frequency and demonstrates distinguishable differences among different concentrations of NaCl in DI water. Measured results for capacitive coupled resonators confirms that increasing the concentration of NaCl in water increases the conductivity of the water and reduces the quality factor, thereby creating an up-shift in f_L (Fig. 8 inset). Additionally, a nonlinear behavior in the resonant frequency is observed which mainly originates from the nonlinearity of the permittivity change in high concentrations of salt in the DI water.[22] It is clear that the proposed capacitive coupled structure has high potential to be used in sensing applications.

In this paper, a microwave-coupled ring resonator has been explored, using various simulations and experiments, for use in high sensitivity sensor applications with wide dynamic range. A comparison of the implemented capacitive and inductive couple mechanisms shows that the capacitive coupling design provides nearly double the sensitivity to permittivity changes that is displayed in the inductive coupled design. Experimental evidence with saline solutions demonstrates that the capacitive coupled mechanism also has greater range, allowing for detection of a greater variation in concentration. The proposed sensor has a simple design and provides a high quality factor at very low fabrication costs and without the use of active devices.

[1]H.-J. Lee, K.-A. Hyun, and H.-I. Jung, "A high-Q resonator using biocompatible materials at microwave frequencies," Appl. Phys. Lett. **104**, 023509 (2014).

[2]A. K. Horestani, J. Naqui, D. Abbott, C. Fumeaux, and F. Martín, "Two-dimensional displacement and alignment sensor based on reflection coefficients of open microstrip lines loaded with split ring resonators," Electron. Lett. **50**, 620–622 (2014).

[3]A. Ebrahimi, W. Withayachumnankul, S. Al-Sarawi, and D. Abbott, "High-sensitivity metamaterial-inspired sensor for microfluidic dielectric characterization," IEEE Sens. J. **14**, 1345–1351 (2014).

[4]H. Torun, F. Cagri Top, G. Dundar, and A. D. Yalcinkaya, "An antenna-coupled split-ring resonator for biosensing," J. Appl. Phys. **116**, 124701 (2014).

[5]H. J. Lee, J. H. Lee, S. Choi, I. S. Jang, J. S. Choi, and H. I. Jung, "Asymmetric split-ring resonator-based biosensor for detection of label-free stress biomarkers," Appl. Phys. Lett. **103**, 053702 (2013).

[6]M. H. Zarifi, M. Rahimi, M. Daneshmand, and T. Thundat, "Microwave ring resonator-based non-contact interface sensor for oil sands applications," Sens. Actuators, B **224**, 632–639 (2016).

[7]H. J. Lee, J. H. Lee, H. S. Moon, I. S. Jang, J. S. Choi, J. G. Yook, and H. I. Jung, "A planar split-ring resonator-based microwave biosensor for label-free detection of biomolecules," Sens. Actuators, B **169**, 26–31 (2012).

[8]H.-J. Lee, H.-S. Lee, K.-H. Yoo, and J.-G. Yook, "DNA sensing using split-ring resonator alone at microwave regime," J. Appl. Phys. **108**, 014908 (2010).

[9]S. Chopra, A. Pham, J. Gaillard, A. Parker, and A. M. Rao, "Carbon-nanotube-based resonant-circuit sensor for ammonia," Appl. Phys. Lett. **80**, 4632 (2002).

[10]C. Bernou, D. Rebière, and J. Pistré, "Microwave sensors: A new sensing principle. Application to humidity detection," Sens. Actuators, B **68**, 88–93 (2000).

[11]A. Sohrabi, P. M. Shaibani, M. H. Zarifi, M. Daneshmand, and T. Thundat, "A novel technique for rapid vapor detection using swelling polymer covered microstrip ring resonator," in *2014 IEEE MTT-S International Microwave Symposium (IMS)* (2014), pp. 1–4.

[12]M. H. Zarifi, A. Mohammadpour, S. Farsinezhad, B. D. Wiltshire, M. Nosrati, A. M. Askar, M. Daneshmand, and K. Shankar, "Time-resolved microwave photoconductivity (TRMC) using planar microwave resonators: Application to the study of long-lived charge pairs in photoexcited titania nanotube arrays," J. Phys. Chem. C **119**, 14358–14365 (2015).

[13]M. H. Zarifi, S. Farsinezhad, M. Abdolrazzaghi, M. Daneshmand, and K. Shankar, "Selective microwave sensors exploiting the interaction of analytes with trap states in TiO₂ nanotube arrays," Nanoscale **8**, 7466–7473 (2016).

[14]A. Ebrahimi, W. Withayachumnankul, S. F. Al-Sarawi, and D. Abbott, "Metamaterial-inspired rotation sensor with wide dynamic range," IEEE Sens. J. **14**, 2609–2614 (2014).

[15]M. H. Zarifi and M. Daneshmand, "Non-contact liquid sensing using high resolution microwave microstrip resonator," in *2015 IEEE MTT-S International Microwave Symposium* (IEEE, 2015), pp. 1–4.

[16]M. H. Zarifi, M. Fayaz, J. Goldthorp, M. Abdolrazzaghi, Z. Hashisho, and M. Daneshmand, "Microbead-assisted high resolution microwave planar ring resonator for organic-vapor sensing," Appl. Phys. Lett. **106**, 062903 (2015).

[17]M. H. Zarifi, S. Farsinezhad, K. Shankar, and M. Daneshmand, "Liquid sensing using active feedback assisted planar microwave resonator," IEEE Microwave Wireless Compon. Lett. **25**, 621–623 (2015).

[18]M. H. Zarifi, T. Thundat, and M. Daneshmand, "High resolution microwave microstrip resonator for sensing applications," Sens. Actuators, A **233**, 224–230 (2015).

[19]U. L. Rohde and A. K. Poddar, "Self-injection locked compact coupled planar resoator based cost-effective ultra low phase noise VCOs for wireless systems," in *2007 18th European Conference on Circuit Theory and Design* (IEEE, 2007), pp. 998–1001.

[20]J.-S. Hong and M. J. Lancaster, "Aperture-coupled microstrip open-loop resonators and their applications to the design of novel microstrip bandpass filters," IEEE Trans. Microwave Theory Tech. **47**, 1848–1855 (1999).

[21]High-Frequency Structure Simulator, see http://www.ansys.com/. HFSS is a commercial finite element method solver for electromagnetic structures from Ansys. It is a commercial tool for antenna design, and the design of complex radio-frequency electronic circuit elements including, transmission lines, and filters.

[22]N. Gavish and K. Promislow, "Dependence of the dielectric constant of electrolyte solutions on ionic concentration," e-print arXiv:1208.5169.